Canadian Science Publishing
NRC Research Press journals | Publishing Services

Canadian Geotechnical Journal
Revue canadienne de géotechnique

Drained cavity expansion analysis with a unified state parameter model for clay and sand

Journal:	*Canadian Geotechnical Journal*
Manuscript ID	cgj-2016-0695.R3
Manuscript Type:	Article
Date Submitted by the Author:	27-Nov-2017
Complete List of Authors:	Mo, Pin-Qiang; China University of Mining and Technology, State Key Laboratory for GeoMechanics and Deep Underground Engineering Yu, Hai-Sui; University of Leeds, School of Civil Engineering
Is the invited manuscript for consideration in a Special Issue? :	N/A
Keyword:	cavity expansion analysis, analytical solution, drained analysis, unified state parameter model, cone penetration test

Drained cavity expansion analysis with a unified state parameter model for clay and sand

Pin-Qiang Mo, Associate Research Scientist

Email: pinqiang.mo@cumt.edu.cn

State Key Laboratory for GeoMechanics and Deep Underground Engineering

School of Mechanics and Civil Engineering, China University of Mining and Technology

No.1 Daxue Road, Xuzhou, Jiangsu, 221116, China

Hai-Sui Yu, Professor of Geotechnical Engineering

and Pro-Vice-Chancellor

Email: PVC.int@leeds.ac.uk

School of Civil Engineering, University of Leeds

Leeds, LS2 9JT, U.K.

submitted on 28 November 2017

approx. 4000 words

14 Figures and 4 Tables

ABSTRACT

This paper presents an analytical solution for drained expansion in both spherical and cylindrical cavities with a unified state parameter model for clay and sand (CASM) (Yu, 1998). The solution developed here provides the stress and strain fields during the expansion of a cavity from an initial to an arbitrary final radius. Small strains are assumed to the elastic region and large strains are applied for soil in the plastic region by using logarithmic strain definitions. Since its development, the unified CASM model has been demonstrated by many researchers to be able to capture the overall soil behaviour for both clay and sand under both drained and undrained loading conditions. In this study, the CASM model is used to model soil behaviour whilst we develop a drained cavity expansion solution with the aid of an auxiliary variable. This is an extension of the undrained solution presented by the authors (Mo and Yu, 2017). The parametric study investigates the effects of various model constants including the stress-state coefficient and the spacing ratio on soil stress paths and cavity expansion curves. Both London clay and Ticino sand are modelled under various initial stress conditions and initial state parameters. The newly-developed analytical solution highlights the potential applications in geotechnical practice (e.g. for the interpretation of cone penetration test (CPT) data) and also serves as useful benchmarks for numerical simulations of cavity expansion problems in critical state soils.

KEYWORDS

Cavity expansion analysis, analytical solution, drained analysis, unified state parameter model, cone penetration test

List of notations provided on Page 3

NOTATION

a	radius of cavity
c	radius of the elastic/plastic boundary
e	void ratio of granular material
m	parameter to combine cylindrical ($m = 1$) and spherical ($m = 2$) analysis
n	stress-state coefficient for CASM
p', q	mean stress and deviatoric stress
p'_0	initial mean effective stress
p'_{y0}	preconsolidation pressure
r	radial position of soil element around the cavity
r^*	spacing ratio for the concept of state parameter
G	elastic shear modulus
K	elastic bulk modulus
R_0	isotropic overconsolidation ratio, defined as p'_{y0}/p'_0
χ	auxiliary independent variable, defined as u/r
δ , γ	volumetric and shear strains
ε_p , ε_q	volumetric and shear strains
ε_r , ε_θ	radial and tangential strains
η	stress ratio, defined as q/p'
μ	Poisson's ratio of soil
v	specific volume, defined as $1 + e$
σ'_r , σ'_θ	radial and tangential stresses
ξ	state parameter
ξ_R	reference state parameter
$M, \kappa, \lambda, \Gamma, \Lambda$	critical state soil parameters

INTRODUCTION

The cavity expansion method and its applications to geotechnical problems have been extensively developed in the last five decades (e.g., Yu 2000). While early research ~~works~~ was mainly focused on the expansion in elastic materials, analytical solutions have been developed using increasingly more sophisticated constitutive soil models (e.g., Palmer and Mitchell 1971; Vesic 1972; Carter et al. 1986; Yu and Houlsby 1991; Collins and Yu 1996; Chen and Abousleiman 2012, 2013, 2016, 2017; Mo et al. 2014; Vrakas and Anagnostou 2014; Mo and Yu 2017). As a result, the solutions have been particularly of interest to geotechnical engineering problems, such as in-situ soil testing, pile foundations, and tunnelling, largely due to their successful applications in providing simple but useful geotechnical solutions.

Perfect plasticity was initially adopted for cavity expansion in soils under either undrained or drained conditions. Total stress analysis of cohesive soil is typically used for the Tresca and von Mises materials, whereas the drained behaviour of soil is modelled by the effective stress analysis for the Mohr Coulomb material. Among the solutions in elastic-perfectly plastic soils, one of the milestones in cavity expansion solutions was provided by Yu and Houlsby (1991), who derived a unified analytical solution of cavity expansion in dilatant elastic-plastic soils, using the Mohr-Coulomb yield criterion with a non-associated flow rule. The large strain analysis in the plastic region, with the aid of a series expansion, was used to derive a rigorous closed-form solution for both cylindrical and spherical cavities. However, to account for the variation of soil strength during cavity expansion, a solution using a strain-hardening/softening plasticity model was clearly necessary.

As the most widely used strain-hardening or softening models in soil mechanics, critical state soil models (Schofield and Wroth 1968) have been used to derive cavity expansion solutions under both drained and undrained conditions in the last two decades (e.g., Collins and Yu 1996; Cao et al. 2001; Chen and Abousleiman 2012, 2013, 2016; Mo and Yu 2017). It should be noted that drained cavity expansion solutions in critical state soils are very limited due to the unknown stress paths and variations of the specific volume during the cavity expansion process. Palmer and Mitchell (1971) were the first to derive an approximate small-strain analytical solution for cylindrical cavity expansion in normally consolidated clay. Similarity solutions for drained cavities from zero initial radius in critical state soils were presented by Collins et al. (1992) and Collins and Stimpson (1994), who provided the limit cavity pressures for both spherical and cylindrical cavities. However, the asymptotic solutions are only valid for large cavity expansion due to the approach of geometric self-similarity. Other similarity solutions were also developed by Russell and Khalili (2002) using the conventional

Mohr-Coulomb failure criterion and a state parameter sand behaviour model with a non-linear critical state line. More recently, semi-analytical solutions for crushable granular materials were proposed by Jiang and Sun (2012) using a new critical state line, with a state-dependent dilantancy and a bounding surface plasticity model. Again, similarity transformation was introduced for the cavity expansion solutions, and plastic deformation was assumed as zero for constant stress ratio.

By abandoning the assumption of similarity, drained solutions for the expansion of cylindrical cavities in the Modified Cam-clay and bounding surface plasticity soils were reported by Chen and Abousleiman (2013, 2016), with the aid of an auxiliary variable in the plastic region, which aims to convert the Eulerian formulation into Lagrangian form. The approach of auxiliary variable is also applied to the proposed drained solutions for the general shear strain hardening/softening Drucker-Prager models (Chen and Abousleiman 2017) and for the unified hardening parameter-based critical state model (Li et al. 2017). However, as pointed out by Yu (1998) among others, it is also true that the conventional critical state models are less suitable for modelling sand behaviour and heavily overconsolidated clays. Hence existing solutions for cavity expansion for a unified critical state soil model for clay and sand are still limited.

In the present paper, an analytical solution for the expansion of both spherical and cylindrical cavities with a unified state parameter model for clay and sand (CASM) (Yu, 1998) is developed. This is an extension of the undrained cavity expansion solutions of Mo and Yu (2017) to drained loading conditions. After introducing the unified state parameter model CASM, the small strain theory is applied in the elastic region, and the large strain assumption is used for soil in the plastic region. The approach of auxiliary variable used by Chen and Abousleiman (2013) is employed for our drained analysis, which is valid for the expansion of either a spherical or a cylindrical cavity in clay or sand material. In this paper, the results of cavity expansion in both London clay and Ticino sand are presented for stress paths and cavity expansion curves. A parametric study is also provided to investigate the effects of the stress-state coefficient and the spacing ratio, as well as the effects of initial stress condition and initial state parameter of the soil. The interpretation of CPT data using the proposed solution is also compared with data from relevant calibration chamber tests.

PROBLEM DESCRIPTION

A spherical or cylindrical cavity with initial radius a_0 in an infinite soil (Fig. 1a) is assumed to be expanded under fully drained conditions. As reported in Mo and Yu (2017), Fig. 1b

schematically illustrates the geometry and kinematics of cavity expansion. The initial stress state is assumed as isotropic, with $\sigma'_{r,0} = \sigma'_{\theta,0} = p'_0$. For the cylindrical case, $\sigma'_{z,0}$ is equal to p'_0, and the effect of σ'_z is not included in this study. For soil with an overconsolidated stress history, the preconsolidation pressure is referred to as p'_{y0}, and $R_0 = p'_{y0}/p'_0$ represents the isotropic overconsolidation ratio in terms of the mean effective stress. The initial specific volume is referred to as v_0, and the specific volume varies during the process of expansion for the drained analysis. Note that a compression positive notation is used throughout this paper, consistent with the undrained solution of Mo and Yu (2017).

For cavity expansion problems, the stresses of soil must satisfy the following quasi-static equilibrium equation:

$$\sigma'_\theta - \sigma'_r = \frac{r}{m}\frac{d\,\sigma'_r}{d\,r} \tag{1}$$

where the parameter 'm' is used to integrate both spherical ($m = 2$) and cylindrical ($m = 1$) scenarios (following Yu and Houlsby 1991, Collins and Yu 1996, and Mo and Yu 2017); σ'_r and σ'_θ are the effective radial and tangential stresses, and r is the radius of the material element (r_0 is the initial position before cavity expansion). The symbol 'd' denotes the Eulerian derivative for every material particle at a specific moment.

According to Collins and Yu (1996), the mean and deviatoric effective stresses (p' ; q) for cavity expansion problems can be defined as follows:

$$\begin{aligned} p' &= \frac{\sigma'_r + m\cdot\sigma'_\theta}{1+m} \\ q &= \sigma'_r - \sigma'_\theta \end{aligned} \tag{2}$$

Accordingly, the volumetric and shear strains (δ ; γ) can be written as:

$$\begin{aligned} \delta &= \varepsilon_r + m\cdot\varepsilon_\theta \\ \gamma &= \varepsilon_r - \varepsilon_\theta \end{aligned} \tag{3}$$

As stated in Mo and Yu (2017), the definitions of 'p'', 'q' provided in eq. (2) and 'δ', 'γ' in eq. (3) are used consistent with the solution of Collins and Yu (1996), which can contribute to the simplification of the analytical solutions. For the problem with an isotropic in-situ stress state, the possible error introduced by this simplification has been shown to be negligible by a rigorous numerical (finite element) simulation (Sheng et al. 2000), which has also been reported by Chen and Abousleiman (2012).

Considering plastic soil behaviour, the strains are decomposed additively into elastic and plastic components. The superscripts 'e' and 'p' are used to distinguish the elastic and plastic

components of the total strains. According to Collins and Stimpson (1994), the deformation in the elastic region is in fact isochoric with no volumetric change, although the material is compressible. Thus, the small strain analysis is used for soil in the elastic region, as expressed:

$$\begin{aligned} \varepsilon_r &= -\frac{d\,u}{d\,r} \\ \varepsilon_\theta &= -\frac{u}{r} \end{aligned} \tag{4}$$

where u is the radial displacement. Conversely, to accommodate the effect of large deformation in the cavity expansion process, the large strain analysis is adopted for the plastic regions by assuming logarithmic strains (which are also termed true strains or Hencky strains):

$$\begin{aligned} \varepsilon_r &= -\ln\left(\frac{d\,r}{d\,r_0}\right) \\ \varepsilon_\theta &= -\ln\left(\frac{r}{r_0}\right) \end{aligned} \tag{5}$$

UNIFIED STATE PARAMETER MODEL

The unified state parameter model (CASM, developed by Yu 1998) is briefly described in this section, which was also provided in Mo and Yu (2017). The critical state line is fully defined as:

$$\begin{aligned} q &= M\,p' \\ v &= \Gamma - \lambda\,\ln p' \end{aligned} \tag{6}$$

where q and p' are the deviatoric and mean effective stresses; M is the slope of the critical state line in $p'-q$ space; $v = 1+e$ is the specific volume, and e is the void ratio; λ, κ and Γ are the critical state constants.

The state parameter ξ is defined by Wroth and Bassett (1965) and Been and Jefferies (1985) as the vertical distance between the current state and the critical state line in $\ln p' - v$ space (see Fig. 2a):

$$\xi = v + \lambda\,\ln p' - \Gamma \tag{7}$$

With benefits of the concept of state parameter, Yu (1998) proposed a unified state parameter model for clay and sand, which is referred to as CASM. The state boundary surface of the CASM is described as:

$$\left(\frac{\eta}{M}\right)^n = 1 - \frac{\xi}{\xi_R} \tag{8}$$

where $\eta = q/p'$ is known as the stress ratio; n is the stress-state coefficient, which is a new material constant and typically ranges between 1.0 ~ 5.0; $\xi_R = (\lambda - \kappa)\ \ln r^*$, is the reference state parameter; and r^* is the spacing ratio, defined as p'_y/p'_x (Fig. 2a). Equation (8) also represents the stress-state relation and the yield function. In terms of the preconsolidation pressure p'_y, the yield surface can be rewritten as follows:

$$\left(\frac{\eta}{M}\right)^n = -\frac{\ln(p'/p'_y)}{\ln r^*} \tag{9}$$

The variation of state boundary surfaces (eq. (9)) with the stress-state coefficient are shown in Fig. 2b, with normalisation of the preconsolidation pressure. Rowe's stress-dilatancy relation (Rowe 1962), as expressed by:

$$\frac{D\ \delta^p}{D\ \gamma^p} = \frac{9\ (M-\eta)}{9+3\ M-2\ M\ \eta} \times \frac{m}{m+1} \tag{10}$$

is adopted to define the plastic potential, which has been widely accepted with greatest success in describing the deformation of sands and other granular media. The symbol 'D' denotes the Lagrangian derivative for a given material particle. The hardening law is then adopted based on a typical isotropic volumetric plastic strain hardening, as shown to be:

$$D\ p'_y = \frac{\nu\ p'_y}{\lambda-\kappa}\ D\ \delta^p \tag{11}$$

It should be noted that the adopted soil model CASM after Yu (1998) could be taken as a basis for further extensions; e.g. to include shear hardening, to include viscoplasticity, for unsaturated soils, for bounded geomaterials, etc. (see Yu, 2006). In terms of a general three-dimensional stress state, M value varying with Lode's angle (proposed by Sheng et al., 2000) could also be included in the yield function, capturing more realistic soil behaviour under various loading paths. This paper, however, focuses on the derivation of drained cavity expansion with the original proposed soil model CASM, largely owing to the simple stress paths of spherical and cylindrical cavity expansion.

ANALYTICAL SOLUTION

The drained analytical solution is provided in this section, for a cavity expanded from a_0 to a. After a certain expansion, the soil medium around the cavity becomes plastic, and the plastic region develops from the cavity wall. The symbol 'c' is the radius of the elastic-plastic boundary; thus, for $r > c$, soil is in the elastic region, and the plastic region is for soil at $a < r < c$ (see Fig. 1).

Solution for soil in the elastic region

To describe the stress-strain relationship in the elastic region, the elastic strain rates are expressed as follows:

$$D\,\delta^e = \frac{1}{K}\,D\,p' \qquad D\,\gamma^e = \frac{1}{2\,G}\,D\,q \tag{12}$$

where K is the elastic bulk modulus, which is equal to $\nu\,p'/\kappa$; G is the elastic shear modulus for an isotropic linear elastic material as defined by Collins and Stimpson (1994), which is determined as:

$$G = \frac{(1+m)\,(1-2\,\mu)\,\nu\,p'}{2\,[1+(m-1)\,\mu]\,\kappa} \tag{13}$$

Based on the assumption of small strains, the distributions of effective stresses in the elastic region can be expressed as follows, according to the solution of Yu and Houlsby (1991):

$$\sigma_r' = p_0' + B_1 \times \frac{1}{r^{1+m}} \qquad \sigma_\theta' = p_0' - B_1 \times \frac{1}{m\,r^{1+m}} \tag{14}$$

where B_1 is a constant of integration. And the distributions of strains in the elastic region can be solved as:

$$\delta = 0 \qquad \gamma = B_2 \times B_1 \times \frac{1+m}{v_0\,p_0'\,m\,r^{1+m}} \tag{15}$$

where $B_2 = [1 + (m-1)\,\mu]\,\kappa/[(1+m)\,(1-2\,\mu)]$. For the elastic stage (i.e. there is no plastic region), B_1 can be derived based on the boundary condition: $\varepsilon_\theta|_{r=a} = -(a-a_0)/a$, which results in $B_1 = v_0\,p_0'\,m\,a^m(a-a_0)/B_2$. However, for the plastic stage, the elastic-plastic boundary is located at $r = c$, and the initial yielding deviatoric stress can be found from the initial yield surface: $q_c = (\ln R_0 / \ln r^*)^{1/n}\,M\,p_0'$. The boundary condition at $r = c$ gives that $B_1 = q_c\,m\,c^{1+m}/(1+m)$ for the plastic stage, and the size of the plastic region c needs to be determined based on the solution for the plastic region.

Solution for soil in the plastic region

Note that for soil in the plastic region ($a < r < c$), the elastic moduli (K and G) are not constants but functions of the mean effective stress p'. The volumetric strain is related to the specific volume: $\delta = -\ln(v/v_0)$. In order to convert the Eulerian formulation (e.g. eq. (1)) to

the Lagrangian description, a suitable auxiliary independent variable, $\chi = u/r = (r - r_0)/r$, is introduced according to Chen and Abousleiman (2013). For the exact solution in the plastic region, numerical integration is required from the elastic-plastic boundary ($r = c$), where the initial yielding conditions are known with $p' = p'_0$, $q = q_c$, $v = v_0$, and $\chi = (c - c_0)/c = B_2\, q_c/[(1+m)\, v_0\, p'_0]$. For a given derivative $D\,\chi$, three formulations need to be established to relate $D\,\chi$ with $D\,p'$, $D\,q$, and $D\,v$, which will be derived from the equilibrium equation, the volumetric strain rate, and the deviatoric strain rate, respectively.

Together with the assumption of large strains (eq. (5)), the expression of strains can be converted into the forms of χ, as follows:

$$\begin{aligned} &\varepsilon_\theta = -\,ln\left(\frac{r}{r_0}\right) = ln(1-\chi) \\ &\varepsilon_r = \delta - m\,\varepsilon_\theta = -\ln\left(\frac{v}{v_0}\right) - m\ ln(1-\chi) = -\,ln\left[\frac{v}{v_0}(1-\chi)^m\right] \\ &\gamma = -\,ln\left[\frac{v}{v_0}(1-\chi)^{m+1}\right] \end{aligned} \tag{16}$$

- *Equilibrium equation*

By using the auxiliary independent variable, the equilibrium equation (eq. (1)) can thus be rewritten as:

$$-q = \frac{r}{m}\frac{D\left(p' + \frac{m}{m+1}q\right)}{D\,\chi}\frac{d\,\chi}{d\,r} \tag{17}$$

and

$$\frac{r\,d\,\chi}{d\,r} = -\frac{u}{r} + \frac{d\,u}{d\,r} = -\chi + \frac{d\,u}{d\,r} \tag{18}$$

where $d\,u/d\,r$ can be obtained from the expression of $\varepsilon_r = ln(1 - d\,u/d\,r)$ together with eq. (16), i.e. $d\,u/d\,r = 1 - v_0/[v\,(1-\chi)^m]$. Therefore, the formulation based on the equilibrium equation is derived as:

$$-q = \frac{D\,p' + \frac{m}{m+1}D\,q}{m\,D\,\chi}\left[1 - \chi - \frac{v_0}{v\,(1-\chi)^m}\right] \tag{19}$$

- *Volumetric strain rate*

The volumetric strain rate in the plastic region indicates the rate of specific volume (i.e. $D\,\delta = -D\,v/\,v$), which is also a combination of elastic and plastic components:

$$D\,\delta = -D\,v/\,v = D\,\delta^e + D\,\delta^p = \kappa \times \frac{D\,p'}{v\,p'} + \frac{\lambda - \kappa}{v}\frac{D\,p'_y}{p'_y} \tag{20}$$

The integration together with the yield criterion (eq. (9)) is equivalent to the expression of the state parameter (eq. (7)), which gives:

$$v = v_0 - \lambda \ln\frac{p'}{p'_0} + (\lambda - \kappa)\left[\ln R_0 - \left(\frac{\eta}{M}\right)^n \ln r^*\right] = C_1 + C_2 \ln p' + C_3\, \eta^n \tag{21}$$

where

$$\begin{aligned} C_1 &= v_0 + \lambda \ln p'_0 + (\lambda - \kappa) \ln R_0 \\ C_2 &= -\lambda \\ C_3 &= -(\lambda - \kappa) \ln r^* / M^n \end{aligned} \tag{22}$$

The derivative form can then be rewritten as:

$$D\, v = C_2 \frac{1}{p'} D\, p' + C_3\, n\, \eta^{n-1}\left(\frac{1}{p'}\, D\, q - \frac{q}{p'^2}\, D\, p'\right) \tag{23}$$

- *Deviatoric strain rate*

Similarly, the deviatoric strain rate is thus further expressed as:

$$D\, \gamma = -\frac{D\, v}{v} + \frac{m+1}{1-\chi}\, D\, \chi = D\, \gamma^e + D\, \gamma^p = B_2 \frac{D\, q}{v\, p'} + \frac{\lambda-\kappa}{v}\, \frac{D\, p'_y}{p'_y}\, \frac{9+3\, M-2\, M\, \eta}{9\, (M-\eta)}\, \frac{m+1}{m} \tag{24}$$

Therefore, the three formulations (eqs. (19), (23), and (24)) provide the increments of $D\, p'$, $D\, q$, and $D\, v$ for a given $D\, \chi$ from $\chi|_{r=c}$ to $\chi|_{r=a} = (a - a_0)/a$. Thus, the distributions of v, χ, stresses and strains in the plastic region are obtained from the numerical integration. The equivalent location of a material particle around the cavity r corresponding to the auxiliary variable χ is revived by integration from a to r:

$$\int_a^r \frac{d\, r}{r} = \ln\frac{r}{a} = \int_{\chi|_{r=a}}^{\chi} \frac{d\, \chi}{1-\chi-v_0/[v\, (1-\chi)^m]} \tag{25}$$

The elastic/plastic boundary c is also obtained from eq. (25) by integration from a to c, which is used to determine B_1 and the distributions in the elastic region (eqs. (14) and (15)).

RESULTS AND DISCUSSION

Validation of the analytical solution

After examining the state boundary surface and the stress-state relation, the Modified Cam-clay model could be accurately recovered by choosing $r^* = 2.0$ and a suitable value of $n \approx 1.5 - 2.0$, as noted by Yu (1998). The validation of the proposed solution is performed by the comparisons of the cylindrical cavity expansion between the recovered Modified Cam-clay analysis and the results of exact analytical solution for the Modified Cam-clay model,

which were reported by Chen and Abousleiman (2013) in conjunction with their drained analysis. The test with an isotropic in-situ stress condition was adopted for R_0 = 3. The parameters were selected to be equivalent to those in Chen and Abousleiman (2013), as summarised in Table 1.

The stress paths, the distributions of stresses and specific volume are presented in Fig. 3, with comparisons of data from Chen and Abousleiman (2013), which was also verified by the finite element simulation. Note that all stress paths presented in this paper are provided for the soil element at the cavity wall. As the solution is quasi-static and time-independent, all soil elements follow the same stress path, but at any stage of the cavity expansion those elements closer to the cavity boundary are further along that path. The present analytical solution is thus validated by the close agreement between the calculated behaviour of the cavity expansion and the verified analytical results, although the Modified Cam-clay model is assumed by matching the state boundary surface and the stress-state relation using the CASM and the differences on the flow rules.

Drained cavity expansion in clay

This section describes the results of drained cavity expansion in clay using the CASM, for both spherical and cylindrical scenarios. Unless stated otherwise, all results are presented by choosing the material constants similar to those of London clay, as suggested by Yu (1998). The soil model parameters and the initial conditions for London clay are listed in Table 2. Note that the frictional constant M is determined by the critical state friction angle, using $M = 2\,(m+1)\,\sin\phi_{cs}\,/[(m+1)-(m-1)\,\sin\phi_{cs}]$; ϕ_{cs} is also assumed based on the triaxial critical state friction: $\phi_{cs} = \phi_{tx}$ for spherical scenario and $\phi_{cs} = 1.125\,\phi_{tx}$ for cylindrical scenario, as suggested by Wroth (1984).

Fig. 4 shows the stress paths in normalised $p' - q$ space for $a/a_0 = 1$ to 10 with the variation of overconsolidation ratio R_0, keeping the initial specific volume constant as 2.0. The critical state lines and initial yield surfaces for the tests with different values of R_0 overlap in normalised $p' - q$ space, and all stress paths start from $q = 0$ and gradually approach the critical state line. The critical state is reached only when the conditions are satisfied: $q/p' = Dq/Dp' = M$. It can be seen that the normalised stresses (i.e. p'/p'_{y0}, $q/(M \cdot p'_{y0})$) increase with the overconsolidation ratio, and slightly higher normalised stresses are found for the spherical tests comparing to the cylindrical tests.

The cavity expansion curves for $a/a_0 = 1$ to 10 are presented in Fig. 5 for both spherical and cylindrical scenarios, respectively; while the variations of the elastic-plastic radius c with the overconsolidation ratio R_0 are shown in Fig. 6. It is clear that the normalised cavity pressure (σ_r'/p_0') increases with the overconsolidation ratio, whereas the elastic-plastic radius appears to be smaller for the test with a higher overconsolidation ratio. The limiting cavity pressure and the constant ratio of c/a are obtained after expansion of approximately 4 times of the initial cavity size, while the cylindrical tests seem to require larger expansion before reaching the limiting values. In addition, comparing to the spherical scenario, the cylindrical tests have lower normalised cavity pressure but larger elastic-plastic radius.

With benefits of the CASM which can be recovered to the Original Cam-clay ($n = 1$ and $r^* = 2.7183$), the effects of model constants n and r^* are investigated by comparing the modelled London clay and the Original Cam-clay. The results of stress paths and cavity expansion curves for both R_0 = 1 and 16 are shown in Figs. 7-8, respectively. The difference on the yield surfaces results in the loci of stresses and cavity expansion curves for both London clay and the Original Cam-clay. Higher normalised stresses and limiting cavity pressure are found for London clay with $R_0 = 1$, whereas the tests of the Original Cam-clay show higher values of normalised stresses and limiting cavity pressure for heavily overconsolidated clay. It is clear that the analytical solution with the CASM can be used for materials with different softening/hardening responses, by modifying the values of stress-state coefficient n and spacing ratio r^*.

Drained cavity expansion in sand

Similarly, the results of drained cavity expansion in sand using the CASM are described in this section, which are presented by choosing the material constants similar to those of Ticino sand, as suggested by Yu (1998). The soil model parameters for Ticino sand and the initial conditions under $p_0' = 200\ kPa$ are listed in Table 3.

To investigate the effect of initial state parameter, ξ_0 from -0.075 to 0.075 is examined under a constant initial mean stress of 200 kPa. Note that $\xi_0 = 0.075$ indicates the initial condition at the normal compression line, since the reference state parameter $\xi_R = 0.075$. The results of the cavity expansion curves and stress paths in $\ln p' - v$ space are presented in Figs. 9-10, respectively. It is shown that the increase of initial state parameter reduces the limiting cavity pressure and increases the limiting specific volume on the critical state line. Comparing to the spherical tests, the value of limiting cavity pressure for the cylindrical scenario is about half of that of the spherical scenario, which also results in a higher specific volume in Fig. 10.

The effect of initial mean stress is also investigated by varying p'_0 from 200 kPa to 800 kPa for ξ_0 of both -0.075 and 0.075. The corresponding soil parameters and the initial conditions are provided in Table 4, and the stress paths in $\ln p' - v$ space are illustrated in Fig. 11 for both spherical and cylindrical scenarios, respectively. Clearly, apart from the initial state parameter, the initial stress condition has a large influence on the stress-strain relationship for soil around the cavity.

Furthermore, the effects of the model constants n and r^* are illustrated in Figs. 12-13, for the results of cavity expansion curves and stress paths in $\ln p' - v$ space, respectively. By varying the stress-state coefficient n between 2 and 4, and the spacing ratio r^* between 108.6 and 1000, different softening responses of sand can be satisfactorily modelled, as suggested by Yu (1998). Thus the responses of cavity expansion in Fig. 12 show that the increase of either n or r^* can reduce the limiting cavity pressure for $\xi_0 = -0.075$, while the limiting cavity pressure increases with n and r^* for $\xi_0 = 0.075$. The stress paths in Fig. 13 present different loci of $\ln p' - v$ relation, while the difference of loci for $\xi_0 = 0.075$ is significantly larger than that of $\xi_0 = -0.075$. Correspondingly, the limiting state of specific volume decreases with n and r^* for $\xi_0 = 0.075$, and the reverse trends are found for $\xi_0 = -0.075$.

Potential geotechnical applications

Note that the proposed solution provides a general approach for drained cavity expansion/contraction problems using the critical state soil models, with the concept of state parameter and two additional soil parameters. The current solution with an arbitrary cavity expansion has major potential applications, including cone penetration tests, pressuremeter tests, pile foundations, tunnelling, and wellbore instability. Moreover, the solution serves as a benchmark for validating numerical simulations of boundary value problems.

A simple example for application to the interpretation of CPT data has been provided here using the developed analytical solution. The cone penetration testing in the calibration chambers is widely accepted as a versatile tool for interpretation between penetration resistance and soil properties. The cone tip resistance q_c is one of the main test measurements, which is usually related to the in situ effective stress and soil density. The approach of spherical cavity expansion idealises the cone penetration as an analogy of the expanded cavity under the same conditions by Vesic (1977) and Yu and Mitchell (1998) amongst many others. The cone resistance can therefore be predicted based on the calculated cavity pressure (Ladanyi and Johnson 1974):

$$q_c = \sigma_r'|_{r=a} \times \left(1 + \sqrt{3}\tan\phi\right) \quad (26)$$

where ϕ is assumed as the critical state friction angle. Thus the relationship between the normalised cone tip resistance Q, defined as $(q_c - p_0')/p_0'$, and the in situ state parameter ξ_0 is provided. The tests with Ticino sand (soil parameters can be found in Table 3) are conducted at an initial effective stress of $p_0' = 74$ kPa (after a test of Ghafhazi and Shuttle 2008). The initial state parameter ξ_0 varies from -0.3 to 0.0, indicating an initial specific volume from 1.58 to 1.88. The results are shown in Fig. 14, with a good comparison with data from the calibration chamber tests (Shuttle and Jefferies 1998; Ghafghazi and Shuttle 2008). The calibration chamber tests cover the initial mean stress in the range $50\,\text{kPa} < p_0' < 500\,\text{kPa}$, and the initial specific volume between 1.5 and 1.9. The results show that the normalised cone tip resistance decreases with the value of initial state parameter, whereas the stress level was found to have little effect on the $Q - \xi_0$ curve. It should be noted that, for application of the proposed solution, further study is required for the back-analysis of CPT data. To estimate the properties of soils based on the limited measured data, other techniques (e.g. probabilistic identification, Wang et al. 2013; statistical characterization, Niazi et al. 2011) are desired to be incorporated into the solution developed in this paper.

CONCLUSIONS

A new analytical solution for drained expansion of both spherical and cylindrical cavities with a unified state parameter model for clay and sand (CASM) (Yu 1998) is proposed in this paper. CASM is a critical state soil model with two additional material constants, which has the ability to capture the overall behaviour of either clay or sand under both drained and undrained loading conditions. The developed cavity expansion solution with large strain analysis provides the entire stress-strain histories of soils in the elastic and plastic regions. The approach of auxiliary variable is employed for our drained analysis, which unifies the spherical/cylindrical scenarios and clay/sand models.

As an illustration, both London clay and Ticino sand are modelled under various initial stress conditions and initial state parameters. The parametric study investigates the effects on stress paths and cavity expansion curves. Higher normalised cavity pressure (σ_r'/p_0') is obtained for the test with a higher overconsolidation ratio, which also results in a smaller elastic-plastic radius. The increase of initial state parameter reduces the limiting cavity pressure but increases the limiting specific volume on the critical state line. The results also show the ability of this solution for modelling materials with different softening/hardening responses by modifying the values of the stress-state coefficient and the spacing ratio. In addition, this

analytical solution provides a general analytical approach for drained cavity expansion problems using other sophisticated critical state soil models. A simple application to the interpretation of CPT data using the proposed solution shows a good comparison with data from the calibration chamber tests. As shown by Yu (2000), it is expected that the new cavity expansion solution developed in this paper can also be applied with success to other relevant geotechnical problems such as pressuremeter tests, pile foundations and tunnelling in clay and sand under drained loading condition.

ACKNOWLEDGMENTS

The authors would like to acknowledge financial support by "the Fundamental Research Funds for the Central Universities" (No. 2017QNB10).

REFERENCES

Been, K. and Jefferies, M.G. 1985. A state parameter for sands. Géotechnique, 35(2): 99–112.

Cao, L.F., Teh, C.I., and Chang, M.F. 2001. Undrained cavity expansion in modified cam clay I: Theoretical analysis. Géotechnique, 51(4): 323–334.

Carter, J.P., Booker, J.R., and Yeung, S.K. 1986. Cavity expansion in cohesive frictional soils. Géotechnique, 36(3): 349–358.

Chen, S.L., and Abousleiman, Y.N. 2012. Exact undrained elasto-plastic solution for cylindrical cavity expansion in modified cam clay soil. Géotechnique, 62(5): 447–456.

Chen, S.L., and Abousleiman, Y.N. 2013. Exact drained solution for cylindrical cavity expansion in modified cam clay soil. Géotechnique, 63(6): 510–517.

Chen, S.L., and Abousleiman, Y.N. 2016. Drained and undrained analyses of cylindrical cavity contractions by bounding surface plasticity. Canadian Geotechnical Journal, 53(9): 1398–1411.

Chen, S.L., and Abousleiman, Y.N. 2017. Wellbore stability analysis using strain hardening and/or softening plasticity models. International Journal of Rock Mechanics & Mining Sciences, 93: 260–268.

Collins, I.F., and Stimpson, J.R. 1994. Similarity solutions for drained and undrained cavity expansions in soils. Géotechnique, 44(1): 21–34.

Collins, I.F., and Yu, H.S. 1996. Undrained cavity expansions in critical state soils. International Journal for Numerical and Analytical Methods in Geomechanics, 20(7): 489–516.

Collins, I.F., Pender, M.J., and Wang, Y. 1992. Cavity expansion in sands under drained loading conditions. International Journal for Numerical and Analytical Methods in Geomechanics, 16(1): 3–23.

Jiang, M.J., and Sun, Y.G. 2012. Cavity expansion analyses of crushable granular materials with state-dependent dilatancy. International Journal for Numerical and Analytical Methods in Geomechanics, 36(6): 723–742.

Li, L., Li, J.P., Sun, D.A., and Gong, W.B. 2017. Unified Solution to Drained Expansion of a Spherical Cavity in Clay and Sand. International Journal of Geomechanics, DOI: 10.1061/(ASCE)GM.1943-5622.0000909.

Mo, P.Q., and Yu, H.S. 2017. Undrained cavity expansion analysis with a unified state parameter model for clay and sand. Géotechnique, 67(6): 503-515. DOI: 10.1680/jgeot.15.P.261.

Mo, P.Q., Marshall, A.M., and Yu, H.S. 2014. Elastic-plastic solutions for expanding cavities embedded in two different cohesive-frictional materials. International Journal for Numerical and Analytical Methods in Geomechanics, 38(9): 961–977.

Niaza, F.S., Mayne, P.W., and Wang, Y.H. 2011. Statistical Analysis of Cone Penetration Tests and Soil Engineering Parameters at the National Geotechnical Experimentation Clay Site, Texas A&M University, Geo-Frontiers 2011, 2998-3007.

Palmer, A.C., and Mitchell, R.J. 1971. Plane strain expansion of a cylindrical cavity in clay. Proceedings of the Roscoe Memorial Symposium, Cambridge, UK: 588–599.

Rowe, P.W. 1962. The stress-dilatancy relation for static equilibrium of an assembly of particles in contact. Proc. Roy. Soc., 267: 500–527.

Russell, A.R., and Khalili, N. 2002. Drained cavity expansion in sands exhibiting particle crushing. International Journal for Numerical and Analytical Methods in Geomechanics, 26(4): 323–340.

Schofield, A.N., and Wroth, C.P. 1968. Critical state soil mechanics. McGraw-Hill, New York, NY, USA.

Sheng, D., Sloan, S.W., and Yu, H.S. 2000. Aspects of finite element implementation of critical state models. Comput. Mech., 26(2): 185-196.

Vesic, A.S. 1972. Expansion of cavities in infinite soil mass. ASCE Journal of Soil Mechanics and Foundations Division 98(SM3), 5–290.

Vrakas, A., and Anagnostou, G. 2014. A finite strain closed-form solution for the elastoplastic ground response curve in tunnelling. International Journal for Numerical and Analytical Methods in Geomechanics, 38: 1131–1148.

Wang, Y., Huang, K., and Cao, Z.J. 2013. Probabilistic identification of underground soil stratification using cone penetration tests. Canadian Geotechnical Journal, 50: 766-776.

Wroth, C.P. 1984. Interpretation of in situ soil tests. Géotechnique, 34(4): 449–489.

Wroth, C.P., and Bassett, N. 1965. A stress-strain relationship for the shearing behaviour of sand. Géotechnique,15(1): 32–56.

Yu, H.S. 1998. CASM: A unified state parameter model for clay and sand. International Journal for Numerical and Analytical Methods in Geomechanics, 22(8): 621–653.

Yu, H.S. 2000. Cavity Expansion Methods in Geomechanics, Kluwer Academic Publishers, Dordrecht, The Netherland.

Yu, H.S. 2006. Plasticity and Geotechnics, Springer, New York, NY, USA.

Yu, H.S., and Houlsby, G.T. 1991. Finite cavity expansion in dilatant soils: loading Analysis. Géotechnique, 41(2): 173–183.

Figure Captions:

Fig. 1. Geometry and kinematics of cavity expansion.

Fig. 2. A general stress-state relation for both clay and sand in: (a) $\ln p' - v$ space; (b) $p'/p'_y - q/(M \cdot p'_y)$ space.

Fig. 3. Comparisons between the proposed solution and results after solution of Chen and Abousleiman (2013) for the Modified Cam-clay model.

Fig. 4. Stress paths for $a/a_0 = 1$ to 10 with variation of overconsolidation ratio ~~of~~ R_0: (a) spherical scenario; (b) cylindrical scenario.

Fig. 5. Cavity expansion curves for $a/a_0 = 1$ to 10 with variation of overconsolidation ratio ~~of~~ R_0: (a) spherical scenario; (b) cylindrical scenario.

Fig. 6. Variations of elastic-plastic radius c for $a/a_0 = 1$ to 10 with overconsolidation ratio ~~of~~ R_0: (a) spherical scenario; (b) cylindrical scenario.

Fig. 7. Effect of model constants n and r^* on stress paths for clay: (a) spherical scenario; (b) cylindrical scenario.

Fig. 8. Effect of model constants n and r^* on cavity expansion curves for clay: (a) spherical scenario; (b) cylindrical scenario.

Fig. 9. Cavity expansion curves for $a/a_0 = 1$ to 10 with variation of initial state parameter ξ_0: (a) spherical scenario; (b) cylindrical scenario.

Fig. 10. Stress paths in $\ln p' - v$ space for $a/a_0 = 1$ to 10 with variation of initial state parameter ξ_0: (a) spherical scenario; (b) cylindrical scenario.

Fig. 11. Stress paths in $\ln p' - v$ space for $a/a_0 = 1$ to 10 with variation of initial mean stress p'_0: (a) spherical scenario; (b) cylindrical scenario.

Fig. 12. Effect of model constants n and r^* on cavity expansion curves for sand: (a) spherical scenario; (b) cylindrical scenario.

Fig. 13. Effect of model constants n and r^* on stress paths in $\ln p' - v$ space for sand: (a) spherical scenario; (b) cylindrical scenario.

Fig. 14. Prediction of the relationship between normalised cone tip resistance and initial state parameter.

Table Headers:

Table 1. Soil model parameters and initial conditions for validation of the proposed solution.

Table 2. Soil model parameters and initial conditions for London clay.

Table 3. Soil model parameters and initial conditions for Ticino sand under $p_0' = 200\ kPa$.

Table 4. Soil model parameters and initial conditions for Ticino sand under $p_0' = 400, 600, 800\ kPa$.

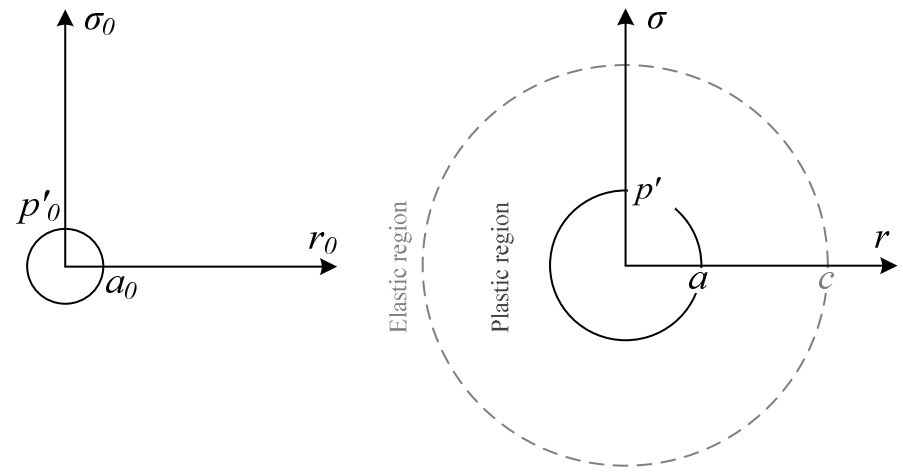

(a) Initial cavity before expansion (b) Cavity after expansion

Fig. 1. Geometry and kinematics of cavity expansion.

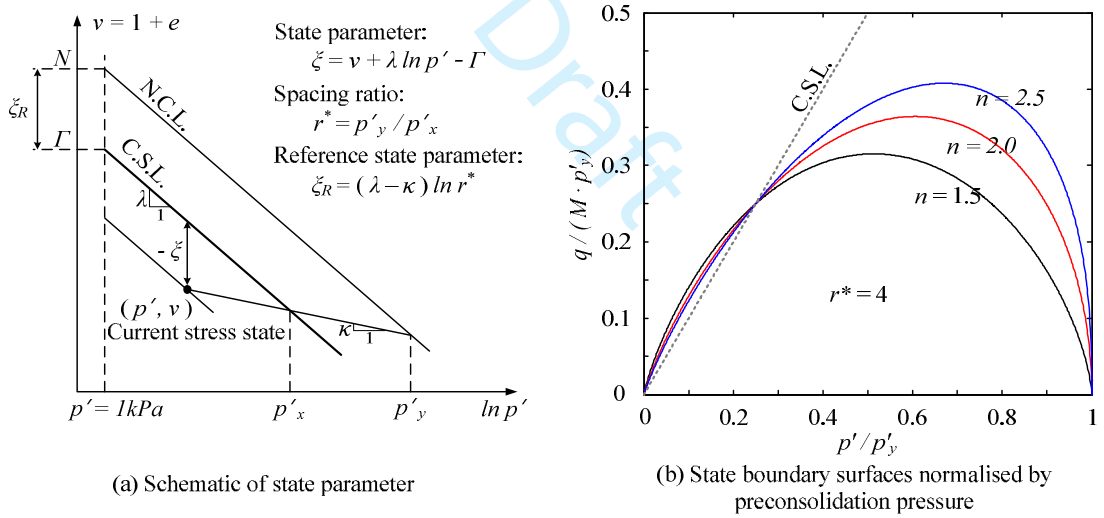

(a) Schematic of state parameter (b) State boundary surfaces normalised by preconsolidation pressure

Fig. 2. A general stress-state relation for both clay and sand in: (a) $\ln p' - v$ space; (b) $p'/p'_y - q/(M \cdot p'_y)$ space.

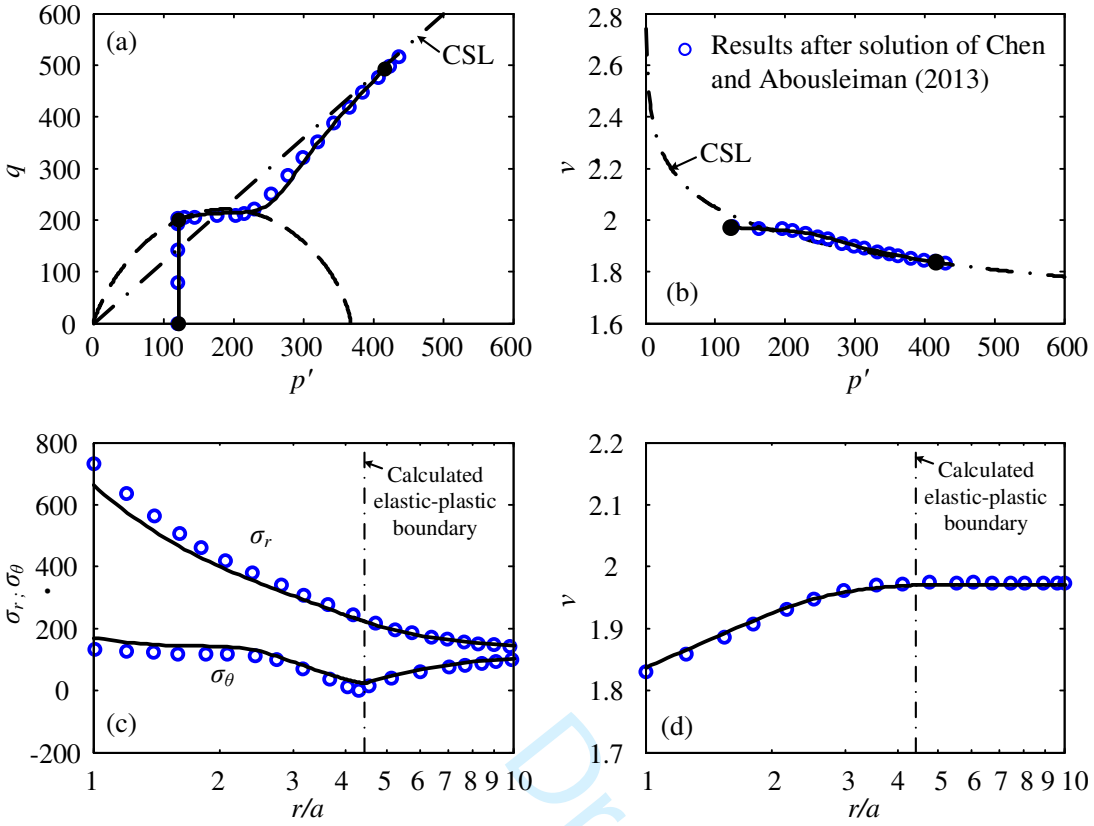

Fig. 3. Comparisons between the proposed solution and results after solution of Chen and Abousleiman (2013) for the Modified Cam-clay model.

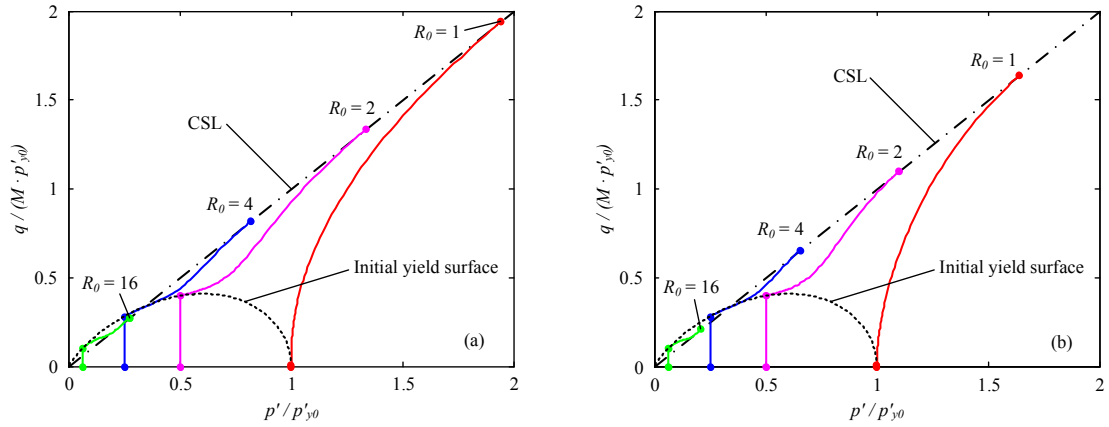

Fig. 4. Stress paths for $a/a_0 = 1$ to 10 with variation of overconsolidation ratio ~~of~~ R_0: (a) spherical scenario; (b) cylindrical scenario.

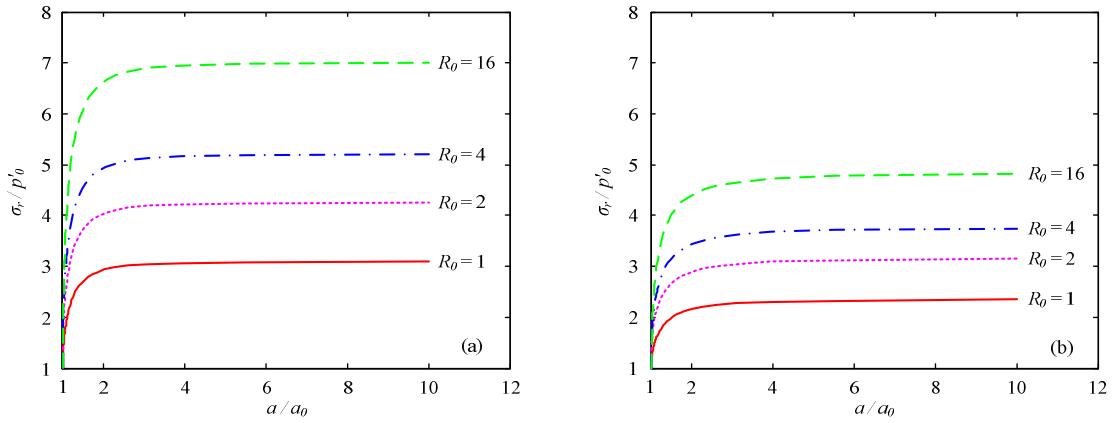

Fig. 5. Cavity expansion curves for $a/a_0 = 1$ to 10 with variation of overconsolidation ratio ~~of~~ R_0: (a) spherical scenario; (b) cylindrical scenario.

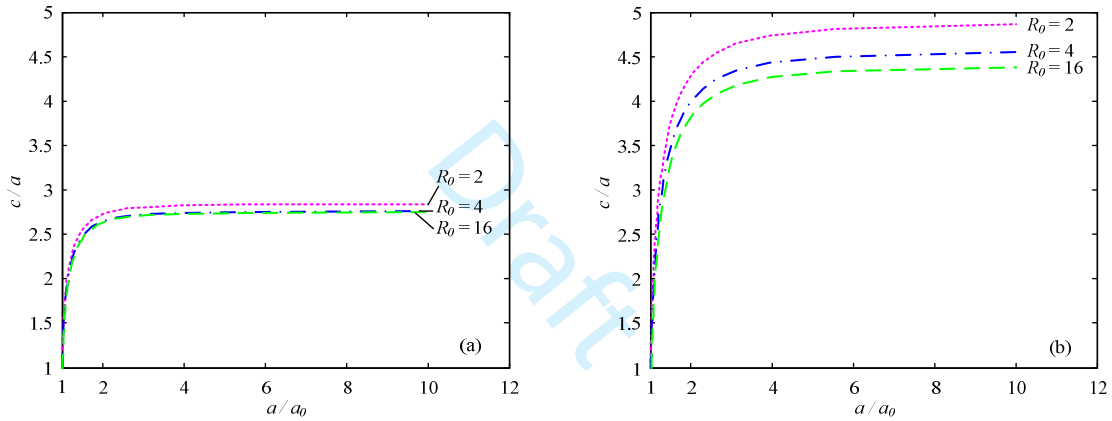

Fig. 6. Variations of elastic-plastic radius c for $a/a_0 = 1$ to 10 with overconsolidation ratio ~~of~~ R_0: (a) spherical scenario; (b) cylindrical scenario.

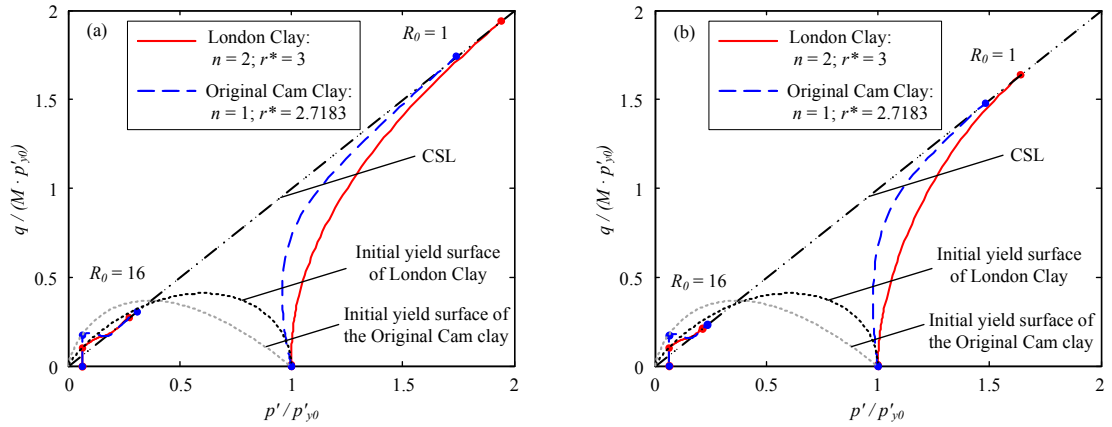

Fig. 7. Effect of model constants n and r^* on stress paths for clay: (a) spherical scenario; (b) cylindrical scenario.

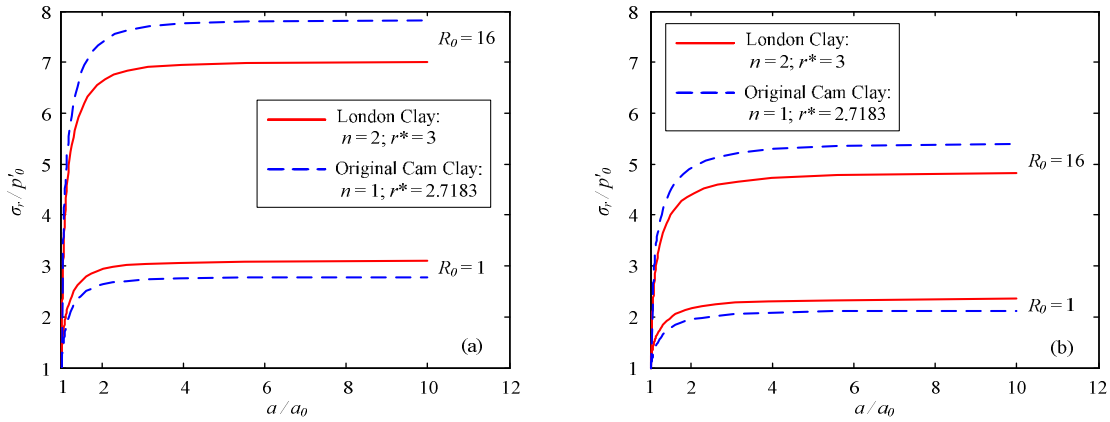

Fig. 8. Effect of model constants n and r^* on cavity expansion curves for clay: (a) spherical scenario; (b) cylindrical scenario.

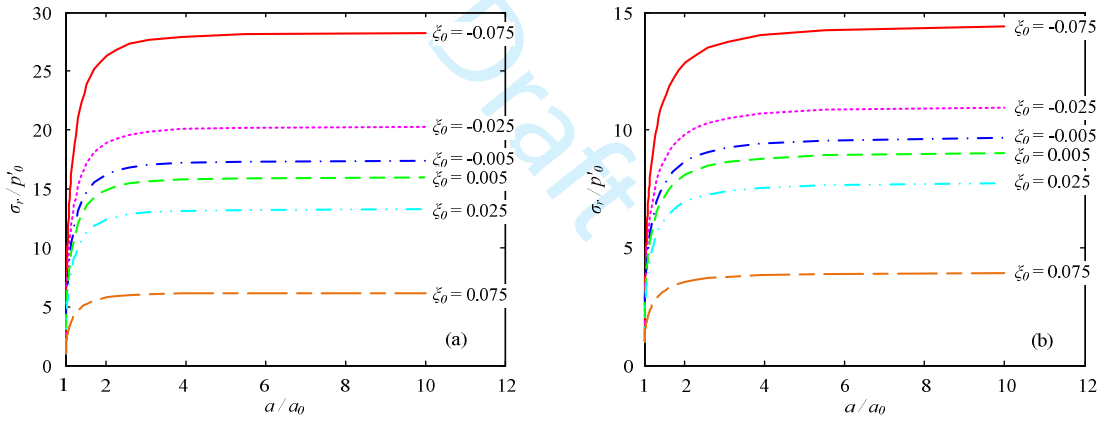

Fig. 9. Cavity expansion curves for $a/a_0 = 1$ to 10 with variation of initial state parameter ξ_0: (a) spherical scenario; (b) cylindrical scenario.

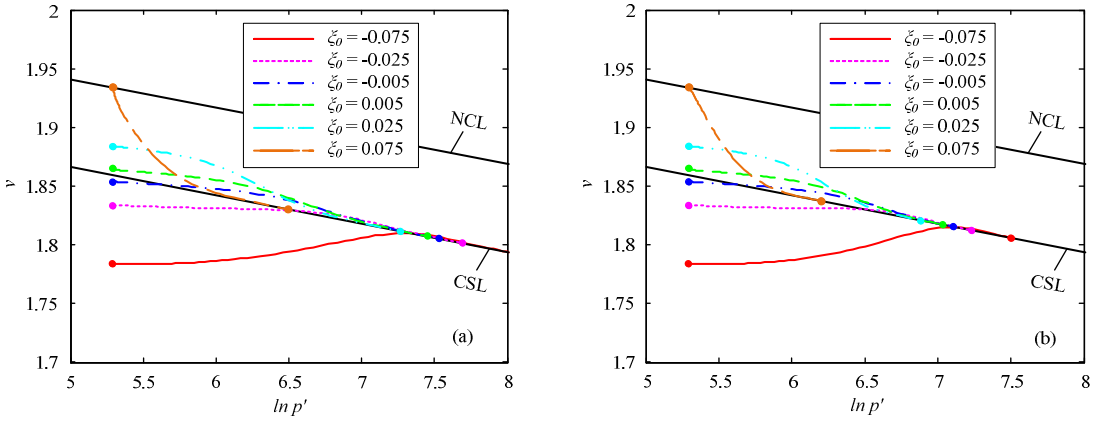

Fig. 10. Stress paths in $\ln p' - v$ space for $a/a_0 = 1$ to 10 with variation of initial state parameter ξ_0: (a) spherical scenario; (b) cylindrical scenario.

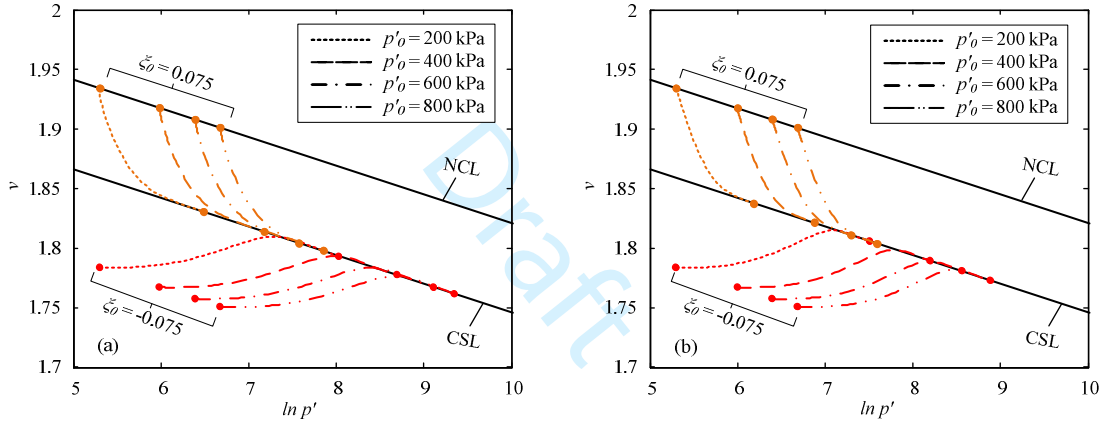

Fig. 11. Stress paths in $\ln p' - v$ space for $a/a_0 = 1$ to 10 with variation of initial mean stress p'_0: (a) spherical scenario; (b) cylindrical scenario.

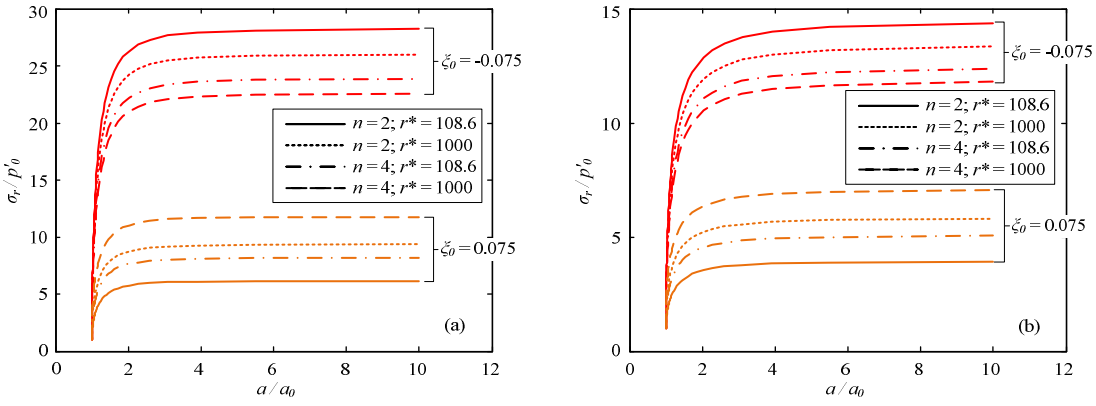

Fig. 12. Effect of model constants n and r^* on cavity expansion curves for sand: (a) spherical scenario; (b) cylindrical scenario.

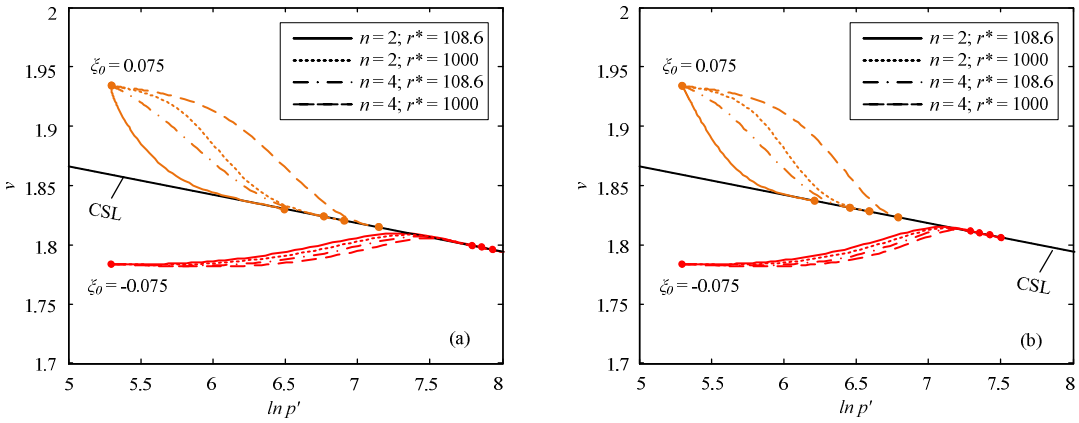

Fig. 13. Effect of model constants n and r^* on stress paths in $\ln p' - v$ space for sand: (a) spherical scenario; (b) cylindrical scenario.

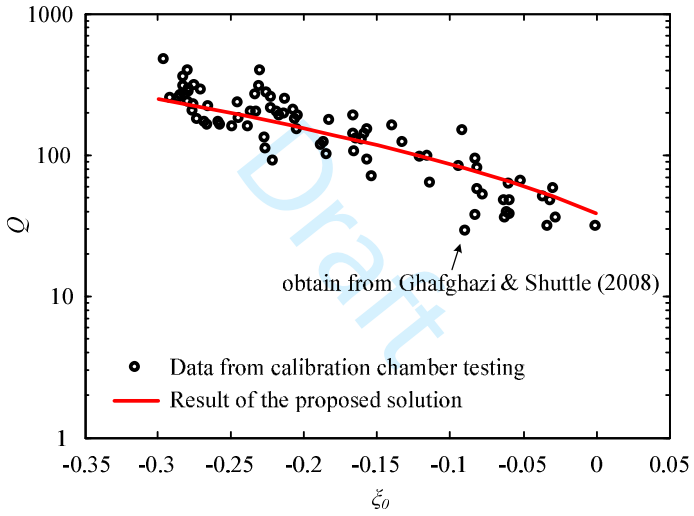

Fig. 14. Prediction of the relationship between normalised cone tip resistance and initial state parameter.

Table 1. Soil model parameters and initial conditions for validation of the proposed solution.

$\Gamma = 2.74;\ \lambda = 0.15;\ \kappa = 0.03;\ \mu = 0.278;\ M = 1.2;\ R_0 = 3;\ \nu_0 = 1.97$		
	This study	Chen and Abousleiman (2013)
Spacing ratio r^*	2.0	-
Stress-state coefficient n	1.5	-
Initial stress p_0' (kPa)	122.6	120
G_0 (kPa)	3575	4113

Table 2. Soil model parameters and initial conditions for London clay.

$\Gamma = 2.759;\ \lambda = 0.161;\ \kappa = 0.062;\ \mu = 0.3; n = 2.0; r^* = 3.0$ $\phi_{tx} = 22.75°: M = 0.8879\ (spherical), M = 0.8640\ (cylindrical)$					
Overconsolidation ratio R_0		1	2	4	6
Initial specific volume ν_0		2.0	2.0	2.0	2.0
Initial stress p_0' (kPa)		219.15	143.11	93.45	39.84
Initial state parameter ξ_0		0.1088	0.0401	-0.0285	-0.1657
G_0 (kPa)	spherical	3263	2131	1391	593
	cylindrical	2828	1847	1206	514

Table 3. Soil model parameters and initial conditions for Ticino sand under $p_0' = 200\ kPa$.

$\Gamma = 1.986;\ \lambda = 0.024;\ \kappa = 0.008;\ \mu = 0.3; n = 2.0; r^* = 108.6$ $\phi_{tx} = 32.0°: M = 1.2872\ (spherical), M = 1.1756\ (cylindrical)$							
Initial state parameter ξ_0		-0.075	-0.025	-0.005	0.005	0.025	0.075
Initial stress p_0' (kPa)		200	200	200	200	200	200
Overconsolidation ratio R_0		11792	518.1	148.4	79.5	22.8	1.0
Initial specific volume ν_0		1.7838	1.8338	1.8538	1.8638	1.8838	1.9338
G_0 (kPa)	spherical	20583	21160	21390	21506	21737	22314
	cylindrical	17838	18338	18538	18638	18838	19338

Table 4. Soil model parameters and initial conditions for Ticino sand under $p_0' = 400, 600, 800\ kPa$.

Initial state parameter ξ_0		-0.075 ($R_0 = 11792$)			0.075 ($R_0 = 1$)		
Initial stress p_0' (kPa)		400	600	800	400	600	800
Initial specific volume v_0		1.7672	1.7575	1.7506	1.9172	1.9075	1.9006
G_0 (kPa)	spherical	40782	60836	80796	44243	66028	87719
	cylindrical	35344	52724	70023	38344	57224	76023